Radio Environment Map Construction by Residual Kriging Based on Generalized Regression Neural Network

Haiyang Xia[1], Song Zha[1], Jijun Huang[1], and Jibin Liu[1]

[1]National University of Defense Technology

November 24, 2022

Abstract

Radio environment map (REM) is an efficient enabler for practical cognitive radio networks by sensing the electromagnetic information within regions of interest dynamically. Most of works on Kriging-based method have proven that separate estimation for pathloss and shadowing can obtain more accurate REM construction. But these methods have some shortcomings that prior information is required for construction or disability for multiple transmitters scenario. In order to overcome the problems of urban REM construction mentioned above, this paper propose a residual Kriging algorithm based on generalized regression neural network (GRNN-RK) for that. The performance of proposed algorithm has been evaluated by the analysis of simulation results, and experiments show that GRNN is capable of improving Kriging in accuracy. Additionally, the influence of spread on REM construction is also experimented.

1

1

Radio Environment Map Construction by Residual Kriging Based on Generalized Regression Neural Network

Haiyang Xia[1], Song Zha[1]†, Jijun Huang[1], Jibin Liu[1]

[1]College of Electronic Science and Engineering, National University of Defense Technology

†Corresponding author: Song Zha (zhasong0551@163.com)

Key Points:

- REM construction for urban area is faced with the problem that no prior information of transmitters or propagation environment can be obtained precisely because of the complicated electromagnetic environment.

- Separated estimation for pathloss and shadowing can guarateen the second order stationarity to improve the accuracy of Kriging method.

- Residual Kriging based on generalized regression neural network performances better than ordinary Kriging in accuracy for urban REM construction in areas of multiple transmitters without any prior information.

Abstract

Radio environment map (REM) is an efficient enabler for practical cognitive radio networks by sensing the electromagnetic information within regions of interest dynamically. Most of works on Kriging-based method have proven that separate estimation for pathloss and shadowing can obtain more accurate REM construction. But these methods have some shortcomings that prior information is required for construction or disability for multiple transmitters scenario. In order to overcome the problems of urban REM construction mentioned above, this paper propose a residual Kriging algorithm based on generalized regression neural network (GRNN-RK) for that. The performance of proposed algorithm has been evaluated by the analysis of simulation results, and experiments show that GRNN is capable of improving Kriging in accuracy. Additionally, the influence of spread on REM construction is also experimented.

1 Introduction

The demand for wireless communication terminals has experienced an incredible increase with the breakthrough in the field of emerging technologies, such as 5G and IoT, in the last decade, which gives rise to the increasing scarcity of spectrum resource(Liu et al. 2017). This phenomenon deteriorates because of the traditional spectrum allocation mechanism, for the static allocation results in unreasonable distribution of spectrum resource(Sun, Wu, and Li 2015). A dynamistic and flexible spectrum allocation mechanism has been required desperately to solve current communication problems.

REMs can be applied in cognitive radio (CR) to solve the problem of spectrum allocation based on its precise awareness of the electromagnetic environment in the spatial or time domain by processing the measurements collected by sample capable devices(Yilmaz Birkan et al. 2013)(Pesko et al. 2014). Apart from spectrum allocation, REMs also have applications in the field of intra operator radio resource management, dedicated spectrum monitoring and electromagnetic pollution prevention(Szmit and Lopatka 2015)(Hu and Zhang 2019). Current REM construction methods can be classified into three types: direct methods, indirect methods and hybrid ones(Pesko et al. 2014)(Yucek and Arslan 2009). Direct methods refer to interpolations based on the measurement merely while indirect methods need more prior information of propagation environment of transmitters(Meshkova et al. 2011)(Alfattani and Yongacoglu 2018), and hybrid ones are the combination of direct and indirect methods(Bolea, Pérez-Romero, and Agustí 2011).

In consideration of the REM construction in the urban areas, in which the information of transmitters and propagation environment is complicated and difficult to obtain precisely(Tanis 2019), improvement of accuracy has been attached to importance because it is directly related to the utilization efficiency of spectrum. Although indirect and hybrid methods outnumber direct methods in accuracy, they are also influenced by the accuracy of the prior information. Since the prior information such as transmitters' locations and transmitting power is too difficult to collect precisely because of the complicated electromagnetic environment and large scale of transmitting terminals, direct methods are the most suitable for urban REM construction according to their stability. Many theoretical and experimental studies have been conducted on REM construction methods(Denkovski et al. 2012)(Umer, Kulik, and Tanin 2010), and Kriging, a geo-statistic interpolation method based on the measurement dataset, is well known because of its good performance in accuracy(Xia et al. 2020)(Han et al. 2019)(Boccolini, Hernandez-Penaloza, and Beferull-Lozano 2012). It minimizes the variance of estimation errors under the

61 constraint of unbiased estimation(Oliver and WEBSTER 1990). And ordinary Kriging (OK) is a
62 basic Kriging method utilized in REM construction widely, which realizes the accurate
63 prediction of spatial random field obeying the Gaussian process through the variogram fitting
64 and Kriging system(Isaaks and Srivastava 1989).

65   In general case of REM, received power strength (RSS)(Pesko et al. 2014)(Flexible and
66 Spectrum Aware Radio Access through Measurements and Modelling in Cognitive Radio
67 Systems 2011) is one of the most widely chosen to describe the electromagnetic field. RSS
68 consists of two components(Erceg et al. 1998)(M Lebreton, Murad, and Lorion 2016): the
69 pathloss component results from the information of transmitters and propagation environment
70 while the shadowing component is derived from the surrounding environment effect. Since
71 shadowing component is a slow fading obeying log-normal distribution(Gudmundson 1991),
72 which can be viewed as a spatial random field. But pathloss is not constant mean in the region of
73 interest, RSS is not second order stationary. So, if Kriging is applied for the shadowing
74 estimation, the pathloss component should be subtracted before that, which is a regression
75 problem of a trend surface fitting problem. The separate estimation can guarantee the
76 prerequisite obeyed, resulting in the improvement of accuracy of Kriging.
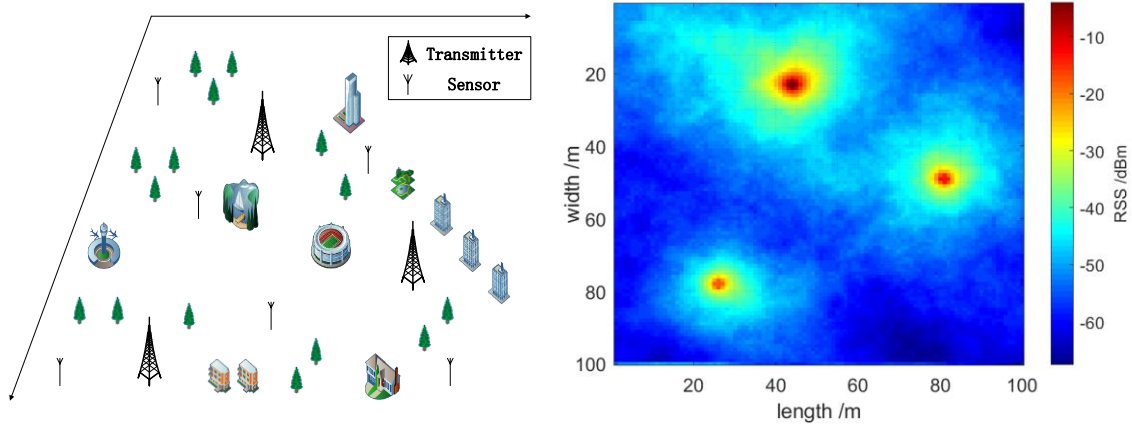
77   Many Kriging-based methods have been proposed for separate estimations. In
78 (Chowdappa et al. 2018), a method estimating the pathloss and shadowing separately is
79 proposed, but parameters of propagation model are required for the regression Kriging(Hengl,
80 Heuvelink, and Rossiter 2007), which is not capable for complicated urban electromagnetic
81 environment. In (Sato 2019), a residual Kriging based on feedforward neural network (FFNN) is
82 provided for REM construction. But it is applied in the situation of only one known transmitter,
83 which cannot be introduced in the multiple transmitters urban area. What is more, radial basis
84 function (RBF)(Park and Sandberg 2014) neural network has better performance the
85 approximation ability, structure simplicity and computation efficiency compared FFNN. Among
86 RBFs, GRNN is a one-pass learning algorithm with a high parallel structure(Specht 1991). Its
87 performance has been tested by providing smooth transitions from one observed value to another
88 with sparse measurements in a multidimensional space. So, GRNN can be utilized to model the
89 pathloss component(Ayadi, Zineb, and Tabbane 2017)(Sotiroudis et al. 2013) and provide the
90 residual measurements for Kriging prediction for the situation of multiple transmitters without
91 any prior information.

92   Therefore, a method of residual Kriging based on generalized regression neural network
93 is put forward to improve the REM construction accuracy in the urban area. The main
94 contribution of this paper is to apply GRNN to process pathloss modeling and residual Kriging
95 for shadowing without any prior information of transmitters or propagation environment. The
96 performance of proposed method has been assessed by the simulation results and mean squared
97 error (MSE)(Azpurua and Dos Ramos 2010) is applied to evaluate the accuracy under different
98 conditions. The variation of spread in GRNN, which is a key parameter controlling the modeling
99 smoothness, has been discussed as well.

100   The rest of this paper is organized as follows. In Section 2, scenario and propagation
101 model of electromagnetic and problem statements are introduced. Section 3 describes the
102 proposed algorithm structure and mechanism in details. In Section 4, simulations and results
103 analysis are discussed. And conclusions are drawn in Section 5.

2 Model and Problem Statement

In this paper, the geographic region of interest is considered as a two dimensional space, denoted by , within which laid a number of active transmitters, whose transmitting power and locations can be denoted by and , respectively. Also, a few sensors are deployed randomly within the same region to collect the electromagnetic field information, e.g. received signal strength (RSS). These sensors constitute a smart terminals network to monitor the region of interest, so their measurements and locations , are known to the REM construction system. The deployment of transmitters and sensors is shown in Figure 1 (a) and the corresponding REM is displayed in Figure 1 (b).

(a) the deployment of transmitters and sensors   (b) corresponding REM

Figure 1 The Region of Interest

Assuming that the fast fading effects are averaged out by multiple measurements, based on the pathloss and shadowing model, for the sensor $s_r(i)$, the RSS (dBm) can be expressed as

$$P_r(i) = P_{r,pl}(i) + V(i) \quad [dBm], \quad (1)$$

$$P_{r,pl}(i) = 10 \log_{10} P_{r,pl,mW}(i) \quad [dBm],$$

where $P_{r,pl}(i)$ is the pathloss component while $V(i)$ is the shadowing component. And the pathloss component is the sum of $P_{r,i,mW}(j)$, each transmitter propagation power in form of W at $s_r(i)$, which is given by

$$P_{r,pl,mW}(i) = \sum_j^m P_{r,i,mW}(j) \quad [W], \quad (2)$$

$$P_{r,i,mW}(j) = 10^{\frac{1}{10}P_{r,i}(j)} \quad [W],$$

where $P_{r,i}(j)$ can be modeled as

$$P_{r,i}(j) = P_t(j) + K + 10\eta \log_{10} d_0 + 10\eta \log_{10} \| s_t(j) - s_r(i) \| \quad [dBm], \quad (3)$$

where $P_t(j)$ is the transmitting power, K is the constant pathloss factor, η is the pathloss exponent, d_0 is a reference distance for antenna far field and $\|\cdot\|$ is the Eulidean distance between two locations.

130　　　　As for the shadowing $V(i)$, it follows a lognormal distribution with a standard deviation,
131　which is a spatially correlated fading, and the Gudmundson model is employed in this paper,
132　which is expressed by

$$133 \quad C(s(i), s(j)) = \sigma_\psi^2 \exp(-\frac{\|s(i) - s(j)\|}{d_c}) \ [dB], \ (4)$$

134　where σ_ψ is the standard deviation and d_c is the correlation distance. The applicability of this
135　model in REM has been empirically tested.

136　　　　The proposed algorithm aims to construct an accurate REM for the region of interest
137　based on dataset, that is to calculate the RSS at all points within the region without any deployed
138　sensor $\{\hat{P}_r \mid \hat{P}_r(i), i = 1, ..., N\}$ according to measurements P_r and deployments s_r of sensors.

3 Algorithm Description

140　　　　In Section 2, the problem of accurate REM construction has been discussed in the
141　scenario raised above, and GRNN-RK is applied to solve this problem. In order to improve the
142　accuracy of REM. GRNN-RK divides the estimation of RSS into two ways: one is GRNN
143　modeling for pathloss component, another is Kriging prediction for shadowing component. And
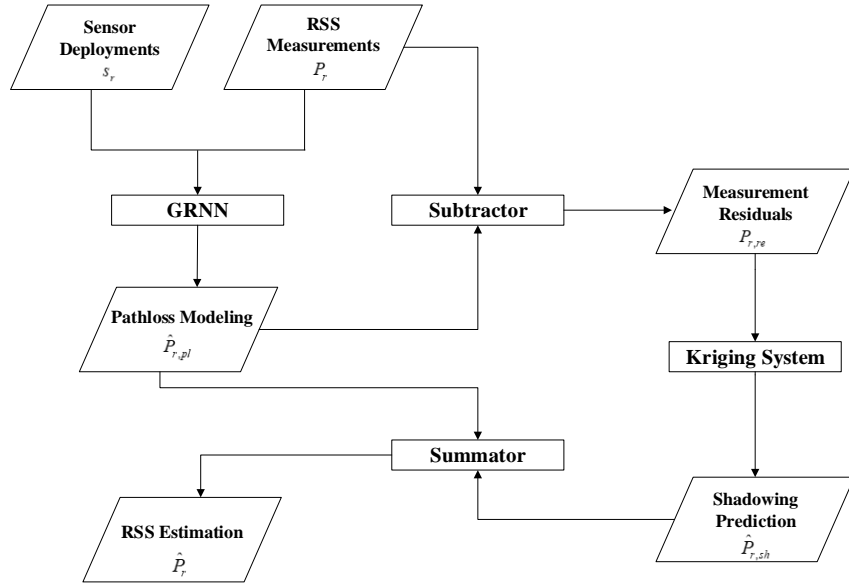144　Figure 2 is the flow chart of GRNN-RK, and it will be described in details below.

145
146　　　　　　　　　　　　　**Figure 2** Flow Chart of GRNN-RK

147　　　　3.1 Pathloss Modeling via GRNN

148　　　　The regression is the essential step of importance because it fits the trend surface of
149　pathloss as well as provides measurement residuals for shadowing prediction. If the modeling
150　results are too similar to the measurements, the accuracy of Kriging prediction will be influenced
151　negatively by the inappropriate measurement residuals. If the modeling results are little similar to
152　the measurements, the gap between results and trend surface is too large to fit the pathloss
153　component. In order to model the pathloss component appropriately, GRNN is selected to fit the
154　trend surface in this paper.
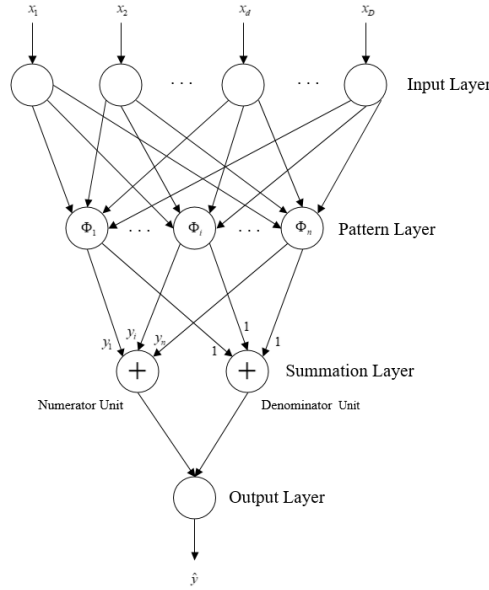
155
156 **Figure 3** GRNN Structure

157   GRNN is a variant of RBF neural network with a one pass learning algorithm and highly
158 parallel structure, which was introduced by Specht in 1991 as a memory-based network. It can
159 provide smooth approximation of a target nonlinear function with sparse sampling values in
160 multiple dimensional space, which is the current challenge of pathloss modeling discussed above
161 in Section 2 as well. What is more, fast learning and easy tuning are also its remarkable
162 advantages.

163   The GRNN is composed of four layers, including the input layer, the pattern layer, the
164 summation layer and the output layer, which is shown in Figure 3. The number of neurons in the
165 input layer equals the dimensions of input vector and their transfer functions are linear functions.
166 The pattern layer of GRNN is radial basis layer, and each neuron inside uses a radial basis
167 function as an activation function, which is commonly taken to be Gaussian. And it is given by

$$\Phi_i(x) = \exp(-\frac{\|x - c_i\|^2}{2\sigma_s^2}) , (5)$$

169 where c_i is a center vector and σ_s is a smoothing parameter controlling the spread of radial basis
170 function. Unlike other layers, the summation layer has two kinds of neurons. One, named as
171 numerator unit, is utilized to calculate the weighted sum of neurons of the pattern layer, another,
172 named as denominator unit, is utilized to calculate the algebraic sum. And output of GRNN is the
173 result of outputs of numerator unit divided by the counterpart of denominator unit, which can be
174 expressed as

$$\hat{y}(x) = \frac{\sum_{i=1}^{n} \Phi_i(x) y_i}{\sum_{i=1}^{n} \Phi_i(x)} . (6)$$

176   In the process of pathloss modeling via GRNN, only one parameter should be set, that is
177 the smoothing parameter σ_s, which is also called the spread of radial basis functions. Spread is a
178 scalar, which has great influence on the smoothness of modeling result. Just as discussed in

179 Section 2, the most critical issue in pathloss modeling is to fit an appropriate smooth trend
180 surface to describe the pathloss component as well as obtain the measurement residuals for
181 Kriging prediction meanwhile. Since the smoothness of modeling represent the accuracy of trend
182 surface, spread should be adjusted to find the optimum value for pathloss modeling.

183 3.2 Shadowing Prediction via Residual Kriging

184 Once the GRNN is constructed, the pathloss component can be obtain from the modeling.
185 Then, the measurement residuals can be calculated by the subtraction of pathloss modeling and
186 sensor measurements, which can be viewed as the samplings of the shadowing component. In
187 consideration of that shadowing obeys lognormal distribution with a zero mean and a standard
188 deviation, Kriging method is applied for its prediction.

189 Kriging, a geo-statistics interpolation introduced by Matheron in 1963, is a Best Linear
190 Unbiased Prediction (BLUE) for spatial random field. Its outstanding performance has been
191 proven in the fields of geographical science, atmospheric science and marine science. The
192 application of Kriging requires the prerequisites that spatial field must be second order stationary
193 or intrinsic, which the shadowing component fulfills.

194 The first step of residual Kriging is variogram fitting based on the measurement residuals.
195 Variogram is used to describe the spatial variability of residuals and to measure the spatial
196 correlation as a function of distance. The empirical variogram is given be

$$\hat{\gamma}(h) = \frac{1}{2|N(h)|} \sum_{N(h)} \left[P_{r,re}(i) - P_{r,re}(j) \right]^2, (7)$$

197

198 where $P_{r,re}(\cdot)$ is the measurement residual, $N(h)$ denotes the set of all location pairs separated
199 by the lag distance h, whereas $|N(h)|$ denotes the number of distinct pairs in $N(h)$. Then, the
200 parametric variogram $\gamma(h)$ can be obtained by fitting the curve of empirical variogram, and it is
201 also a function of distance to describe the spatial variability.

202 Next, Kriging prediction of shadowing component can be viewed as a weighted averagers
203 of measurement residuals, which is expressed by

$$\hat{P}_{r,sh}(s(k)) = \sum_{i=1}^{n} \omega_i(s(k)) \cdot P_{r,re}(i), (8)$$

204

205 where $s(k)$ denotes an unknown point without sensor within the region of interest, $\omega_i(k)$ is the
206 weight of the residual $P_{r,re}(i)$ for the prediction of point k. These weights fulfill the unbiased
207 conditions of the estimator, and they can be obtained by solving a set of linear equations known
208 as the Kriging system, which is given by

$$\sum_{i=1}^{n} \omega_i(s(k)) \cdot \Gamma(s_r(i), s_r(j)) + L(k) = \gamma(s_r(i), s(k)), j = 1, 2, ..., n, (9)$$

209

210 where $\Gamma(s_r(i), s_r(j))$ is the parametric variogram value between sensors located at $s_r(i)$ and
211 $s_r(j)$, $L(\cdot)$ denotes the Lagrange multiplier guaranteeing the universality condition, and
212 $\gamma(s_r(i), s(k))$ is the parametric variogram value between $s_r(i)$ and $s(k)$. The Kriging system
213 also can be expressed in form of matrices

214
$$\begin{bmatrix} \Gamma(s_r(1),s_r(1)) & \Gamma(s_r(1),s_r(2)) & \cdots & \Gamma(s_r(1),s_r(n)) & 1 \\ \Gamma(s_r(2),s_r(1)) & \Gamma(s_r(2),s_r(2)) & \cdots & \Gamma(s_r(2),s_r(n)) & 1 \\ \vdots & \vdots & \ddots & \vdots & \vdots \\ \Gamma(s_r(n),s_r(1)) & \Gamma(s_r(n),s_r(2)) & \cdots & \Gamma(s_r(n),s_r(n)) & 1 \\ 1 & 1 & \cdots & 1 & 0 \end{bmatrix} \cdot \begin{bmatrix} \omega_1(s(k)) \\ \omega_2(s(k)) \\ \vdots \\ \omega_n(s(k)) \\ L(k) \end{bmatrix} = \begin{bmatrix} \gamma(s_r(1),s(k)) \\ \gamma(s_r(2),s(k)) \\ \vdots \\ \gamma(s_r(n),s(k)) \\ 1 \end{bmatrix}. \quad (10)$$

215 The minimized estimation variance of prediction referred to as Kriging variance, is given
216 by

217
$$\sigma^2(s(k)) = \sum_{i=1}^{n} \omega_i(s(k)) \cdot \gamma(s_r(i),s(k)) + L(k). \quad (11)$$

218 3.3 Comprehensice Descriptioin of GRNN-RK

219 GRNN-RK is a comprehensive method which divides the estimation process into
220 pathloss modeling as well as shadowing prediction according to the characteristics of different
221 component. In order to solve the problem of nonlinear function approximation in pathloss
222 modeling, GRNN is applied to obtain the trend surface of pathloss component. Moreover,
223 Kriging prediction is utilized to applied for the lognormal distributional shadowing component.

224 First of all, the RSS measurements P_r are collected by the sensors. And the locations and
225 measurements of sensors will be sent to the GRNN as the input data. According to the spread of
226 radial basis function, GRNN can output the pathloss modeling $\hat{P}_{r,pl}$ to fit the trend surface of
227 pathloss component. Next, measurement residuals $P_{r,re}$ will be obtained by the subtractor based
228 on $\hat{P}_{r,pl}$ at sensors' locations and P_r, which has great influence on the Kriging prediction of
229 shadowing component. Then, the $P_{r,re}$ will be set as the input data to fit the variogram and solve
230 the Kriging system to obtain $\hat{P}_{r,sh}$. The last step is to make the algebraic sum of $\hat{P}_{r,pl}$ and $\hat{P}_{r,sh}$ as
231 the RSS estimation result $\hat{P}_{r,sh}$. The process of GRNN-RK algorithm is displayed in the Table 1.

232 Table 1 The Pseudocode of GRNN-RK

Algorithm Residual Kriging based on Generalized Regression Neural Network
// P_r: RSS measurements // $\hat{P}_{r,pl}$: pathloss component modeling // $P_{r,re}$: measurement residuals // $\hat{P}_{r,sh}$: shadowing component prediction // $\hat{P}_r$: RSS estimation

I:	**Pathloss Modeling via GRNN**
1:	Obtain the $\hat{P}_{r,pl}$ from P_r via GRNN.
2:	Calculate the $P_{r,re}$ from the subtractor based on $\hat{P}_{r,pl}$ and P_r.
II:	**Shadowing Prediction via Residual Kriging**
1:	Compute the empirical and parametric variogram based on $P_{r,re}$.
2:	Obtain the $\hat{P}_{r,sh}$ by solving the Kriging system through the parametric variogram and $P_{r,re}$.
III	**Summation of Component Estimation**

1:	Compute the $\hat{P}_r$ by the summator according to $\hat{P}_{r,pl}$ and $\hat{P}_{r,sh}$.

4 Simulation **and Performance Evaluation**

In order to evaluate the performance of GRNN-RK in accuracy, this section present the comparisons of different methods on different conditions, and MSE is chosen as the assessment criteria, which is defined as

$$MSE = \frac{1}{K}\sum_{k=1}^{K}\left[\hat{P}_r(k) - P_r(k)\right]^2, \quad (12)$$

where K is the number of total unknown point within the region of interest, $\hat{P}_r(\cdot)$ and $P_r(\cdot)$ are the estimation and true value of RSS, respectively. Simulations are processed 100 times on the PC with a processor of AMD Ryzen 7 2700X, 16 gigabytes of memory and Windows 7 ultimate operating system. And the parameters settings are displayed in Table.

Table 2 Parameter Settings of Scenario

Parameter	**Value**
Field dimension	100 m × 100 m
Signal transmission power	30 dBm, 27dBm, 24dBm
Signal frequency	2000 MHz
Path-loss exponent	3
Path-loss for 1 m distance	38 dB

4.1 Performance Test with Different Number of Measurements

Since sampling ratio is a factor of importance in the field of REM construction, the influence of number of measurements on the performance of GRNN-RK is worth consideration as well. It has been proven that GRNN-RK has better performance than GRNN under the same situation in the discussion above, so OK and GRNN-RK will be compared as followed. Figure 4 is the comparison of OK and GRNN-RK on the conditions of different numbers of measurements.
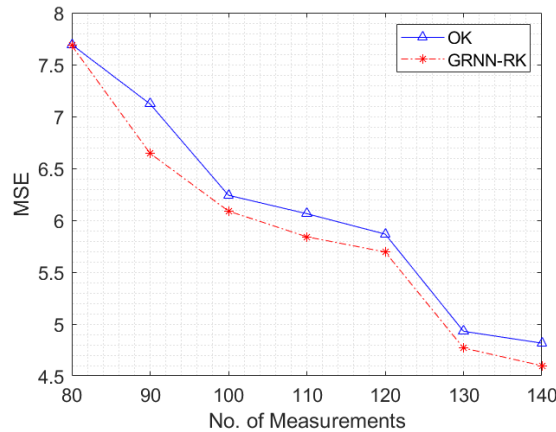

Figure 4 MSE versus No. of Measurements, when $spread = 12$, $\sigma_\psi = 8dB$, $d_c = 15m$

Figure 4 shows that both MSEs decrease with the increase of number of measurements. And MSE of OK is less than that of GRNN-RK when number of measurements is less than 80

254 while GRNN-RK is less than OK after that. What is more, the gap between OK and GRNN-RK
255 also increase. The figure has illustrated that the performance of GRNN-RK is not always better
256 than OK, especially when sampling ratio is less than 0.8% (80 measurements in the region with
257 100×100 points). GRNN-RK's superiority to OK is positively associated with the number of
258 measurements. This demonstrates that the modeling performance of GRNN is essentially based
259 on the number of measurements, and the better modeling GRNN processes, the better
260 improvement residual Kriging make compared to OK.

261   4.2 Performance Test with Different Correlation Distances

262   The performance of two methods in the situations of different correlation distances is
263 analyzed below. From Figure 5, GRNN-RK always performances better than OK. And both
264 methods have less MSE with the increase of correlation distance, but the rate of descent
265 decreases gradually while the gap between two methods increases. The Figure 5 has shown that
266 GRNN-RK performance better than OK in accuracy, and the former can fit for the large
267 correlation distance better.
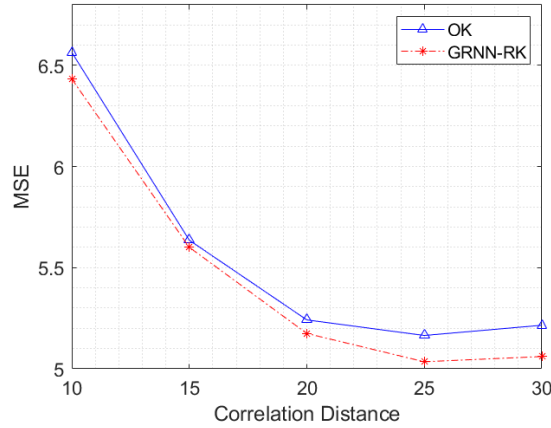268

269
270 **Figure 5** MSE versus Correlation Distance, when $n = 100$, $spread = 12$, $\sigma_\psi = 8dB$

271   4.3 Performance Test with Different Standard Deviations

272   The performance of two methods in the situations of different standard deviation is
273 discussed in this subsection. Figure 6 is MSE versus Standard Deviation, which shows that both
274 methods become less accurate with the increase of standard deviation. When standard deviation
275 is less 3, OK obtains less MSE than GRNN-RK. What is more, even during the deviation range
276 of 3 to 12 dB, the gap between MSEs of OK and GRNN-RK experiences an increase till reaching
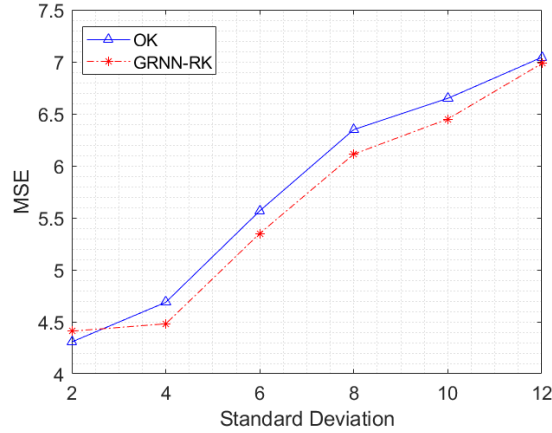277 the peak when deviation is 8 dB, and then it continues to decrease.

278
279 **Figure 6** MSE versus Standard Deviation, when $n = 100$, $spread = 12$, $d_c = 15m$

280 The Figure 6 has demonstrated that, for a specific value of spread, the improvement of
281 GRNN-RK toward OK rises with the increase of deviation at first and then declines. When the
282 standard deviation is small, the effect of shadowing component on RSS is small. Since GRNN
283 aims to fit the trend surface of pathloss, it will emphasize importance on the smoothness to
284 obtain the residual measurements, which has too small contribution to estimation because effect
285 of shadowing component is too small. Under this condition, residual Kriging performs worse
286 than OK. When the standard deviation is large, the effect of pathloss components is small. So
287 residual measurements will have little difference from sensor measurements, performances of
288 residual Kriging and OK will be similar. Therefore, the spread needs to be adjusted to fit for the
289 situations of different standard deviation to improve the performance of GRNN-RK.

290 4.4 Performance Test with Different Spreads

291 After discussions of the relation between scenario parameters the proposed algorithm, the
292 influence of algorithm parameter is also need to be analyzed. The impact of spread on the MSE
293 is shown in Figure 7. In order to analyze the importance of spread adjustment on the pathloss
294 modeling, both of MSEs of GRNN and GRNN-RK estimations are compared in this simulation.
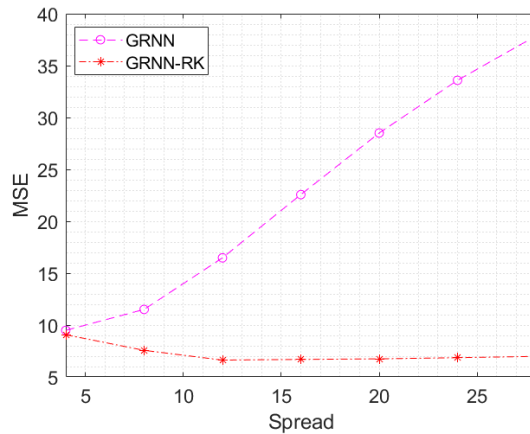

295
296 **Figure 7** MSE versus Spread, when $n = 100$, $\sigma_\psi = 8dB$, $d_c = 15m$

297 From the Figure 7, MSE of GRNN increases sharply with the increase of spread while
298 that of GRNN-RK decreases firstly then reaches its bottom when spread is 12 but it increases

299 slightly with the spread after that. Both MSEs are similar when spread is 4, but their gap begins
300 to increase when spread is getting larger. Just as mentioned in Section 3, the spread controlling
301 the smoothness of the pathloss modeling is a significant parameter needs to choose a suitable
302 value.

303 If the spread is too small, the pathloss modeling will focus on too many details of
304 shadowing component, which leads to that measurement residuals are not accurate enough to
305 support the Kriging prediction. Taking spread equals 4 as an example. In this case, MSE of
306 GRNN is minimum, 9.49, compared to those with a larger spread, but MSE of GRNN-RK
307 reaches its maximum value 9.06. Both of their performance is worse than that of GRNN-RK
308 with a larger spread.

309 If the spread is too large, the modeling will ignore the details of trend surface, which
310 results in that measurement residuals remain too much pathloss component, and cannot meet the
311 requirements of second order stationarity. Obviously when spread equals 28 is a suitable
312 example to illustrate this situation. In this case, MSE of GRNN reaches its peak 37.86, the
313 maximum value without doubts. And MSE of GRNN-RK is 6.98, not its minimum value, which
314 is still slightly larger than 6.62, the minimum MSE obtained by GRNN-RK when spread is 12.
315 The comparisons of true surface of RSSs and pathloss modeling with different spreads are shown
316 in Figure 8.

317
318 (a) true surface of RSS   (b) spread = 4   (c) spread = 8   (d) spread = 12

319
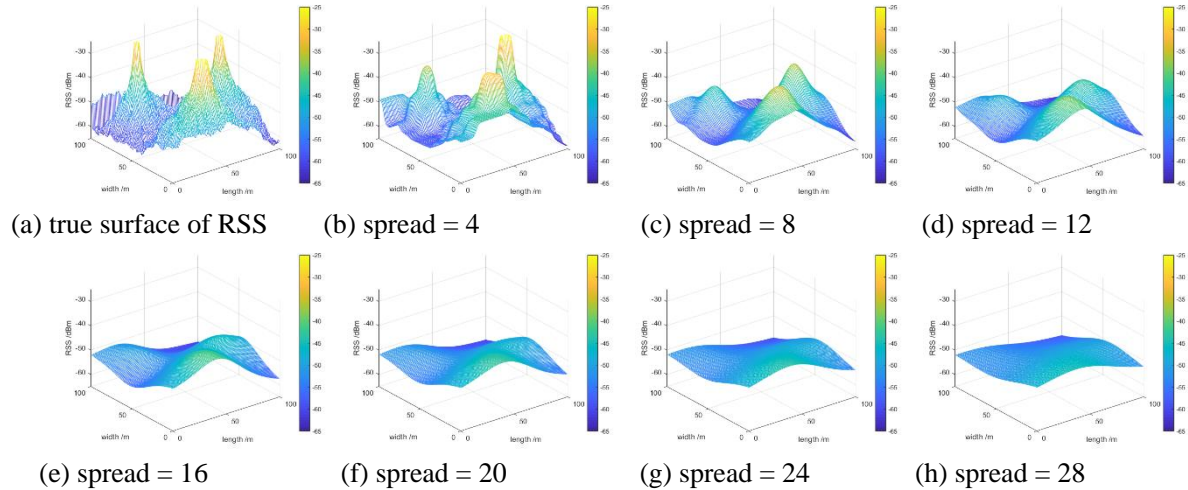320 (e) spread = 16   (f) spread = 20   (g) spread = 24   (h) spread = 28
321 **Figure 8** Comparisons of True Surface of RSSs and Pathloss Modeling with Different Spreads

322 The simulation results demonstrate that GRNN has great influence on the pathloss
323 modeling, which will affect the measurement residuals to control the Kriging prediction results.
324 And the spread is a key parameter controlling the modeling smoothness needs to be adjusted to
325 solve problems under different scenarios. In this case, 12 is the most suitable value for spread to
326 guarantee GRNN-RK has the optimal performance for REM construction. And the true REM and
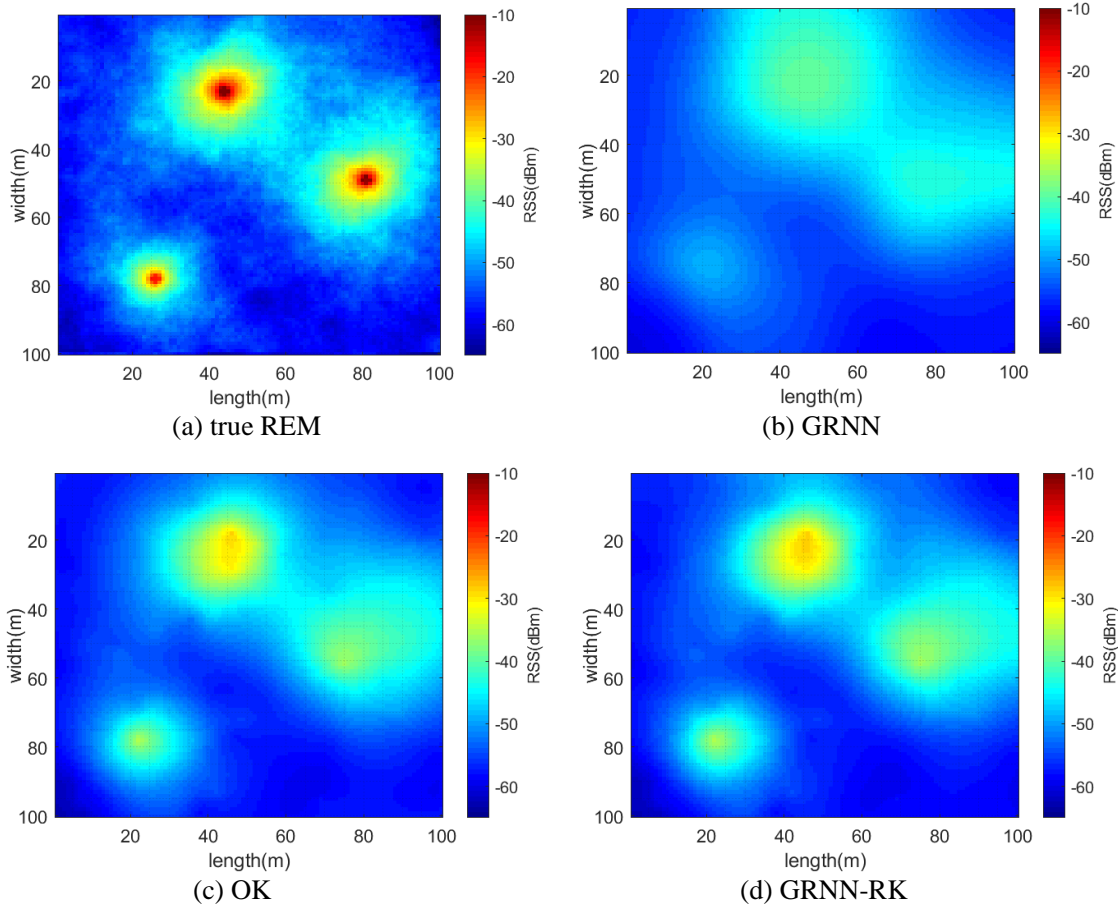327 constructions of different methods are displayed in Figure 9.

328
329   (a) true REM   (b) GRNN

330
331   (c) OK   (d) GRNN-RK
332
333   **Figure 9 the True REM and Constructions of Different Methods**

5 Conclusions

335   In this paper, for constructing highly accurate REM in multiple transmitters region in
336   urban area without any prior information, an algorithm, which applies GRNN for pathloss
337   modeling and residual Kriging for shadowing prediction, has been proposed. Separate estimation
338   can guarantee the second order stationarity of residual measurements to improve the construction
339   accuracy of Kriging. The proposed algorithm is able to construct the highly accurate REM in the
340   urban area of multiple transmitters without any prior information of transmitters or propagation
341   environment. The performance of GRNN-RK has been proven to be better than Kriging in
342   accuracy, and the superiority increase with the increase of sampling ratio and correlation
343   distance. The influence of spread is also analyzed through the experiments. It is a key parameter
344   controlling the smoothness of pathloss modeling, contributing to the prediction accuracy of
345   residual Kriging, but it is also sensitive to standard deviation of shadowing component. Our
346   future work aims at the experience of GRNN-RK on the datasets collected by the spectrum
347   analyzer.

Acknowledgments

354 **References**

355 Alfattani, S., & Yongacoglu, A. (2018). Indirect Methods for Constructing Radio Environment
356 Map. In *2018 IEEE Canadian Conference on Electrical & Computer Engineering (CCECE)* (pp.
357 1–5).
358 Ayadi, M., Zineb, A. Ben, & Tabbane, S. (2017). A UHF Path Loss Model Using Learning
359 Machine for Heterogeneous Networks. *IEEE Transactions on Antennas and Propagation*, *65*(7),
360 3675–3683.
361 Azpurua, M., & Dos Ramos, K. (2010). A comparison of spatial interpolation methods for
362 estimation of average electromagnetic field magnitude. *Progress In Electromagnetics Research
363 M*, *14*(September), 135–145.
364 Boccolini, G., Hernandez-Penaloza, G., & Beferull-Lozano, B. (2012). Wireless sensor network
365 for Spectrum Cartography based on Kriging interpolation. In *IEEE International Symposium on
366 Personal*.
367 Bolea, L., Pérez-Romero, J., & Agustí, R. (2011). Received signal interpolation for context
368 discovery in Cognitive Radio. In *2011 The 14th International Symposium on Wireless Personal
369 Multimedia Communications (WPMC)* (pp. 1–5).
370 Chowdappa, V., Botella, C., Samper-zapater, J. J., & Martínez, R. J. (2018). Distributed Radio
371 Map Reconstruction for 5G Automotive. *IEEE Intelligent Transportation Systems Magazine*,
372 *SUMMER 201*, 36–49. https://doi.org/10.1109/MITS.2018.2806632
373 Denkovski, D., Atanasovski, V., Gavrilovska, L., Riihijarvi, J., & Mahonen, P. (2012).
374 Reliability of a Radio Environment Map: Case of Spatial Interpolation Techniques. In *Cognitive
375 Radio Oriented Wireless Networks and Communications (CROWNCOM)* (pp. 248–253).
376 https://doi.org/10.4108/icst.crowncom.2012.248452
377 Erceg, V., Greenstein, L., Tjandra, S. Y., Parkoff, S. R., Gupta, A., Kulic, B., … Jastrzab, R.
378 (1998). An empirically-based path loss model for wireless channels in suburban environments. In
379 *IEEE JSAC* (Vol. 17, pp. 922–927). https://doi.org/10.1109/GLOCOM.1998.776865
380 *Flexible and Spectrum Aware Radio Access through Measurements and Modelling in Cognitive
381 Radio Systems*. (2011). *European FP-7 project FARAMIR reports*.
382 Gudmundson, M. (1991). Correlation model for shadow fading in mobile radio systems.
383 *Electronics Letters*, *27*(23), 2145–2146.
384 Han, Z., Liao, J., Qi, Q., Sun, H., & Wang, J. (2019). Radio Environment Map Construction by
385 Kriging Algorithm Based on Mobile Crowd Sensing. *Wireless Communications and Mobile
386 Computing*, *2019*(1), 1–12. https://doi.org/10.1155/2019/4064201
387 Hengl, T., Heuvelink, G. B. M., & Rossiter, D. G. (2007). About regression-kriging: From
388 equations to case studies. *Computers & Geosciences*, *33*(10), 1301–1315.
389 Hu, Y., & Zhang, R. (2019). Differentially-Private Incentive Mechanism for Crowdsourced
390 Radio Environment Map Construction. In *IEEE INFOCOM 2019 - IEEE Conference on
391 Computer Communications* (pp. 1594–1602).
392 Isaaks, E. H., & Srivastava, R. M. (1989). An Introduction to Applied Geostatistics. *Oxford
393 University Press, New York*. https://doi.org/10.1080/00401706.1991.10484886
394 Liu, J., Wan, J., Bi, Z., Wang, Q., & Qiu, M. (2017). A Scalable and Quick-Response Software
395 Defined Vehicular Network Assisted by Mobile Edge Computing. *IEEE Communications*

Magazine, *55*(7), 94–100.

M Lebreton, J., Murad, N., & Lorion, R. (2016). Radio Frequency Mapping using an Autonomous Robot: Application to the 2.4 GHz Band. *IOP Conference Series: Materials Science and Engineering*, *120*(1), 12001. https://doi.org/10.1088/1757-899X/120/1/012001

Meshkova, E., Ansari, J., Denkovski, D., Riihijarvi, J., Nasreddine, J., Pavloski, M., … Mahonen, P. (2011). Experimental spectrum sensor testbed for constructing indoor Radio Environmental Maps. In *Proc. of 2011 IEEE Int. Symposium on Dynamic Spectrum Access Networks (DYSPAN 2011)* (pp. 603–607).

Oliver, M. A., & WEBSTER, R. (1990). Kriging: a method of interpolation for geographical information systems. *International Journal of Geographical Information Systems*, *4*(3), 313–332.

Park, J., & Sandberg, I. (2014). Universal Approximation Using Radial-Basis-Function Networks. *Neural Computation*, *3*(2), 246–257.

Pesko, M., Javornik, T., Košir, A., Štular, M., & Mohorčič, M. (2014). Radio environment maps: The survey of construction methods. *KSII Transactions on Internet and Information Systems*, *8*(11), 3789–3809. https://doi.org/10.3837/tiis.2014.11.008

Sato, K. (2019). On the Performance of Neural Network Residual Kriging in Radio Environment Mapping. *IEEE Access*, *7*, 94557–94568. https://doi.org/10.1109/ACCESS.2019.2928832

Sotiroudis, S. P., Goudos, S. K., Gotsis, K. A., Siakavara, K., & Sahalos, J. N. (2013). Application of a Composite Differential Evolution Algorithm in Optimal Neural Network Design for Propagation Path-Loss Prediction in Mobile Communication Systems. *IEEE Antennas and Wireless Propagation Letters*, *12*, 364–367.

Specht, D. . (1991). A General Regression Neural Network. *IEEE Transactions on Neural Networks*, *2*(6), 568–576. https://doi.org/10.1109/IJCNN.2007.4371258

Sun, W. Q., Wu, J. P., & Li, H. W. (2015). Survey on spectrum management in broadband wireless networks. *Ruan Jian Xue Bao/Journal of Software*, *26*(4), 927–944. https://doi.org/10.13328/j.cnki.jos.004812

Szmit, G., & Lopatka, J. (2015). Optimization of Cognitive Radio networks performance using policies definition. In *2015 International Conference on Military Communications and Information Systems (ICMCIS)* (pp. 1–7).

Tanis, S. (2019). Automotive Radar and Congested Spectrum: Potential Urban Electronic Battlefield. *Microwave Journal*, *62*(1), 48,50,52,54,56,58.

Umer, M., Kulik, L., & Tanin, E. (2010). Spatial interpolation in wireless sensor networks: localized algorithms for variogram modeling and Kriging. *GeoInformatica*, *14*(1), 101.

Xia, H., Zha, S., Huang, J., & Liu, J. (2020). Radio environment map construction by adaptive ordinary Kriging algorithm based on affinity propagation clustering. *International Journal of Distributed Sensor Networks*, *16*(5). https://doi.org/10.1177/1550147720922484

Yilmaz Birkan, H., Tugcu, T., Alagöz, F., & Bayhan, S. (2013). Radio environment map as enabler for practical cognitive radio networks. *IEEE Communications Magazine*, *51*(12), 162–169. https://doi.org/10.1109/MCOM.2013.6685772

Yucek, T., & Arslan, H. (2009). A survey of spectrum sensing algorithms for cognitive radio applications. *IEEE Communications Surveys & Tutorials*, *11*(1), 116–130130.